© 2025 Journal of Pharmacy & Pharmacognosy Research, 13 (6), 1728-1741, 2025
ISSN 0719-4250
https://jppres.com

DOI: https://doi.org/10.56499/jppres24.2310_13.6.1728

Original Article

Accelerated bone defect closure after administration of nano bovine hydroxyapatite-calcium sulfate-gelatin scaffold in bone defect models

[Cierre acelerado de defectos óseos después de la administración de un andamio de nano hidroxiapatita bovina-sulfato de calcio-gelatina en modelos de defectos óseos]

Yusuf Alif Pratama[1], Ita Pramudia Ananta[2], Muhammad Shofwan Haris[3], Nuril Maghfiroh[1], Hawin Nabila[1], Chrismawan Ardianto[1], Mahardian Rahmadi[1], Junaidi Khotib[1], Esti Hendradi[4], Muhammad Taher[5], Sakinato Mazidda[6], Aniek Setiya Budiatin[1*]

[1]Department of Pharmacy Practice, Faculty of Pharmacy, Universitas Airlangga, Surabaya, East Java, Indonesia.
[2]Master Program of Pharmaceutical Sciences, Faculty of Pharmacy, Universitas Airlangga, Surabaya, East Java, Indonesia.
[3]Universitas Noor Huda Mustofa, Bangkalan, East Java, Indonesia.
[4]Department of Pharmaceutical Sciences, Faculty of Pharmacy, Universitas Airlangga, Surabaya, East Java, Indonesia.
[5]Department of Pharmaceutical Technology , Kulliyyah of Pharmacy, International Islamic University Malaysia, Kuantan, Pahang, Malaysia.
[6]Department of Physics, Faculty of Science and Technology, Universitas Airlangga, Surabaya, East Java, Indonesia.
*E-mail: aniek-s-b@ff.unair.ac.id

Abstract

Context: Bone defects associated with fractures exceeding 2 cm in circumference present significant clinical challenges due to the high risk of nonunion or malunion. Scaffold implantation offers a non-toxic, effective strategy to support bone regeneration and restore structural integrity.

Aims: To evaluate and compare the regenerative effects of bovine hydroxyapatite-calcium sulfate-gelatin (BHA-CS-gelatin) and nano-BHA-CS-gelatin scaffolds. Focus was placed on cellular morphology, including osteoblasts, osteocytes, and osteoclasts, cell migration, and the expression of osteogenic markers: collagen type I (COL1), Runx2, osteocalcin, and osteoprotegerin (OPG).

Methods: *In vivo* experiments used New Zealand White rabbits with surgically induced bone defects treated with either BHA-CS-gelatin or nano-BHA-CS-gelatin scaffolds. Bone regeneration was assessed by histological, immunohistochemical, and ELISA analyses. Rabbits were sacrificed on days 7 and 28 for histology and immunohistochemistry evaluations. OPG levels were measured by ELISA on days 0, 1, 3, 5, 7, 14, and 28.

Results: Histological analysis showed enhanced migration of osteoblasts, osteocytes, and osteoclasts in the nano-BHA-CS-gelatin group. Immunohistochemistry revealed significantly higher expression of COL1, Runx2, and osteocalcin in this group at day 28 ($p<0.05$). ELISA demonstrated a significant increase in OPG levels on day 14 compared with the conventional BHA-CS-gelatin scaffold group ($p<0.05$).

Conclusions: Nano-BHA-CS-gelatin scaffolds significantly accelerate bone defect closure and enhance osteogenic marker expression more effectively than conventional scaffolds. These results support their preclinical potential application in bone repair and regenerative medicine.

Keywords: bone; bone remodelling; calcium sulfate; nano bovine hydroxyapatite; noncommunicable diseases; scaffold.

Resumen

Contexto: Los defectos óseos resultantes de fracturas, especialmente aquellas con pérdida de circunferencia ósea superior a 2 cm, plantean desafíos significativos debido al riesgo de pseudoartrosis o mala unión. La implantación de andamios ofrece una estrategia no tóxica y eficaz para favorecer la regeneración ósea y restaurar la integridad estructural.

Objetivos: Evaluar y comparar los efectos regenerativos de los andamios de hidroxiapatita bovina-sulfato de calcio-gelatina (BHA-CS-gelatina) y nano-BHA-CS-gelatina. Se centró en la morfología celular, incluyendo osteoblastos, osteocitos y osteoclastos, la migración celular y la expresión de marcadores osteogénicos: colágeno tipo I (COL1), Runx2, osteocalcina y osteoprotegerina (OPG).

Métodos: Experimentos *in vivo* con conejos blancos de Nueva Zelanda con defectos óseos inducidos quirúrgicamente, tratados con andamiajes de gelatina de BHA-CS o de nano-BHA-CS. La regeneración ósea se evaluó mediante análisis histológicos, inmunohistoquímicos y ELISA. Los conejos fueron sacrificados los días 7 y 28 para las evaluaciones histológicas e inmunohistoquímicas. Los niveles de OPG se midieron mediante ELISA los días 0, 1, 3, 5, 7, 14 y 28.

Resultados: El análisis histológico mostró una mayor migración de osteoblastos, osteocitos y osteoclastos en el grupo tratado con nano-BHA-CS y gelatina. La inmunohistoquímica reveló una expresión significativamente mayor de COL1, Runx2 y osteocalcina en este grupo el día 28 ($p<0,05$). La prueba ELISA demostró un aumento significativo en los niveles de OPG el día 14 en comparación con el grupo tratado con el andamio convencional de BHA-CS-gelatina ($p<0,05$).

Conclusiones: Los andamios de nano-BHA-CS-gelatina aceleran significativamente el cierre de defectos óseos y mejoran la expresión de marcadores osteogénicos con mayor eficacia que los andamios convencionales. Estos resultados respaldan su posible aplicación en la reparación ósea clínica y la medicina regenerativa.

Palabras Clave: andamio; enfermedades no transmisibles; hidroxiapatita bovina nano; óseo; remodelación ósea; sulfato de calcio.

ARTICLE INFO
Received: December 4, 2024.
Accepted: July 23, 2025.
Available Online: August 22, 2025.

AUTHOR INFO
ORCID:
0000-0003-2920-6881 (YAP)
0009-0005-9670-1454 (IPA)
0009-0000-5715-4850 (MSH)
0000-0003-3713-7900 (CA)
0000-0002-7256-2446 (MR)
0000-0002-8468-8441 (JK)
0000-0001-9413-1607 (EH)
0000-0002-1463-3090 (MT)
0000-0002-1227-9817 (SM)
0000-0002-1897-4159 (ASB)

Abbreviations: ALP: Alkaline Phosphatase; BHA: Bovine Hydroxyapatite; COL1: Type I Collagen; CS: Calcium Sulfate; EDX: Energy Dispersive X-Ray Spectroscopy; HA: Hydroxyapatite; HE: Hematoxylin & Eosin, IRS: Immunoreactive Score; OPG: Osteoprotegerin; SD: Standard Deviation; SEM: Scanning Electron Microscopy; WHO: World Health Organization.

INTRODUCTION

Bone defects are caused by bone tumors, fractures, osteonecrosis, osteomyelitis, osteoarthritis, trauma, and other diseases (Lu et al., 2021). Continuous structural damage to bone can lead to defects characterized by loss of bone tissue, vascular disruption, and fibrotic tissue formation surrounding the injury site (Smrke et al., 2013; Tang et al., 2016). Fracture is an injury associated with high treatment costs, loss of community productivity, and individual disability (Ghiasi et al., 2017). According to data from the World Health Organization (WHO) in 2020, approximately 35–40% of fracture cases require surgery. A 2018 Indonesia Basic Health Research study reported that 5.5% of patients who suffered fractures in Indonesia experience defects requiring surgery (Kementerian Kesehatan Republik Indonesia, 2018). This is more frequent in fractures that occur in the femur, spine, and facial bones. Under these conditions, biomaterials that serve as bone substitutes (bone grafts) are required to improve medical treatment, thereby reducing functional disabilities caused by bone defects. New medical treatments for fractures can be developed by improving implantation techniques (Song et al., 2018; Stewart et al., 2015), which can provide minerals to fractured bones. Conventional implants made from non-biodegradable materials often require subsequent surgical removal, leading to prolonged recovery times. In contrast, biodegradable scaffolds offer an alternative to integrate with tissue and degrade naturally (Brahimi et al., 2022; Lee et al., 2023).

Scaffolds, serving as three-dimensional matrices used in bone tissue engineering to stimulate the attachment and proliferation of osteoinducible cells on their surfaces (Ghassemi et al., 2018). Bone scaffolds are expected to be osteoconductive (providing a migration pathway for cellular elements such as mesenchymal cells, osteoblasts, and osteoclasts, as well as additional blood vessels) and osteoinductive (inducing cell differentiation into active osteoblasts) (Budiatin et al., 2014; Kazimierczak and Przekora, 2020). Therefore, producing a scaffold with suitable properties for cell penetration, capillary growth, and adequate solute transport that also possesses favorable mechanical and biological properties requires suitable materials. Recently, hydroxyapatite (HA) has emerged as a good material for scaffolds (Baino et al., 2015; Budiatin et al., 2025).

HA, with the chemical formula $Ca_{10}(PO_4)_6(OH)_2$, has a chemical structure similar to that of the inorganic components of the bone matrix and is used as a bone substitute (Adhikara et al., 2024). The biocompatible and tissue-acceptable nature of hydroxyapatite makes it useful as a raw material for biomaterials that can treat, add to, or replace tissue, especially bone tissue (Kamal et al., 2013; Ulery et al., 2011). However, inorganic bioactive materials are fragile, which makes it impossible for them to be used alone in load-bearing applications (Lambert et al., 2017). Therefore, polymers must be added to increase the strength of materials (Jokanović et al., 2017). Gelatin is a denatured collagen polymer, similar to the organic components of bones, that is used to increase the strength of HA. In addition, the use of calcium sulfate to fill bone defects increases bone formation and, for certain indications, can provide results comparable to those of autografts (Yashavantha et al., 2013). Calcium sulfate (CS) has been extensively investigated due to its distinctive physicochemical and biological properties, such as biocompatibility, osteoconductivity, and biodegradability, which provide considerable advantages compared to other bone graft materials (Lun et al., 2024). However, CS is subject to rapid resorption by osteoclasts, potentially leading to an imbalance between material degradation and new bone formation. For a graft material to be considered suitable, its resorption rate must be synchronized with the rate of osteogenesis to ensure optimal mechanical stability. To address this limitation, CS and HA have been combined with polymers to enhance both mechanical strength and controlled degradation of the graft (Tsuchiya et al., 2018; Yan et al., 2014).

The osteoconductive and osteointegrative properties of bone grafts are related to their porosity and pore size. The bone is built and structured by nanocomposites consisting of HA nanocrystals dispersed in an organic matrix, which may offer improved functional and biological properties compared to conventional microstructured biomaterials or composites (Farbod et al., 2014; Khotib et al., 2022). HA-gelatin nanoscaffolds reportedly enhance osteoblast function, as indicated by increased alkaline phosphatase (ALP) activity, calcium deposition, and formation of mineralized bone nodules (Azami et al., 2012). In another study, HA-gelatin nanoscaffolds reportedly modulate dendritic arm formation and significantly increase CD44 gene expression, a marker of osteoblast differentiation into osteocytes (Lee et al., 2013). Nanofibrous scaffolds offer a large surface area, resulting in high reactivity to cellular and molecular components.

While previous studies have evaluated HA or CS individually or in binary combinations, there remains limited research on nano-BHA-based composite scaffolds incorporating CS and gelatin in a nanostructured format. The synergistic interaction between these components is hypothesized to improve osteoinduction and scaffold degradation while maintaining structural integrity.

Therefore, this study aims to evaluate the physicochemical properties and *in vivo* osteogenic potential of a nano-BHA–calcium sulfate–gelatin composite scaffold as a novel platform for bone regeneration.

MATERIAL AND METHODS

Materials

Materials used included BHA (PT. Inobi, Surabaya, Indonesia), calcium sulfate (Elam Pharma Pvt. Ltd., Ankleshwar, Gujarat, India), gelatin (Sigma-Aldrich, St. Louis, MO, USA), xylazine (Xyla; Interchemie, Venray, Netherlands), ketamine (PT. Dexa Medica, Cikarang, Indonesia), ampicillin (PT. Meiji, Jakarta Selatan, Indonesia), and Povidon (PT. Afi Farma, Kediri, Indonesia). Antibodies used include those to Runx, osteocalcin, osteoprotegerin, and type I collagen (Antibodies-online, Limerick, PA, USA).

Animals

The animal trials were approved by the Veterinary Ethics Committee of the Faculty of Veterinary Medicine, Universitas Airlangga (No. 2.KEH.181.12.2023) and were conducted in accordance with the guidelines of the Institutional Regulations for Animal Trials and the Basic Guidelines for Good Animal Experimental Behaviour. The animals were acclimated for one week before the experiment, and all animals were provided with free access to food and water.

This study utilized 30 female white rabbits bred at the animal laboratory, Faculty of Pharmacy, Universitas Airlangga, New Zealand. The animals were aged 4–8 months and weighed between 2.0 and 3.0 kg. The rabbits were randomly assigned to three groups, each consisting of ten individuals (n = 10 per group). The first group served as the control group and did not receive a scaffold; the second group was given a BHA-CS-gelatin scaffold, and the third group was provided with a nano-BHA-CS-gelatin scaffold.

Preparation of the scaffold

The nano-BHA was prepared by mixing 900 mg of BHA and 100 mg of gelatin with 10 mL of distilled water at 50°C (Suyatno et al., 2024). The suspension was sonicated six times using an ultrasonicator for 30 minutes. Microgels with a size of 0.2–0.3 mm were added to the suspension while stirring at 600 rpm for 6 hours under cold conditions. The microgels were used to reduce the particle size of BHA to nano-BHA. The suspension and microgels were separated through filtration. The supernatant was then dried using freeze-drying for 3–4 days at a constant cooling rate of 1°C/min to a final freezing temperature of −55°C to obtain a dry form (Haris et al., 2025; Jakubowska et al., 2022). The scaffold is made by slowly dripping at 40°C until a homogeneous paste is formed. The paste is then dried to form pellets.

Characterization of the scaffold

Scanning electron microscopy (SEM) with energy dispersive X-ray spectroscopy (EDX)

The surface morphology and elemental composition of the scaffolds were examined using scanning electron microscopy (SEM) coupled with energy-dispersive X-ray spectroscopy (EDX). Scaffold samples were sliced to a size of 5 mm (width) × 3 mm (height), sputter-coated with silver, and examined at magnifications of 10,000× and 15,000×. Scale bars were added to each image. Elemental spectra were used to calculate the Ca/P ratio. The results were compared to those of similar studies to assess structural similarity to native bone (Loh and Choong, 2013).

Effectiveness of in vivo scaffold

Thirty New Zealand white rabbits were randomly assigned to three groups: negative control, BHA-CS-gelatin scaffold, and nano-BHA-CS-gelatin scaffold. Each group was further subdivided into two observation timepoints (7 and 28 days; n = 5 per subgroup) (Suyatno et al., 2024). A bone defect model was created by drilling a cylindrical hole (4.2 mm in diameter and 2.0 mm in depth) into the distal femur, followed by scaffold implantation. Postoperative care was provided until wound closure to minimize the risk of infection.

At each designated timepoint (days 7 and 28), the animals were sacrificed, and femurs were harvested and decalcified in 10% EDTA solution (pH 7.4). Bone healing progression was assessed using computed tomography (CT), and defect area measurements were obtained with visible scale bars and magnification annotations.

Histological evaluation using hematoxylin-eosin (HE) staining was conducted to observe the morphology and distribution of osteoblasts, osteoclasts, and osteocytes under 100× magnification

(scale bar: 200 µm). Immunohistochemical (IHC) staining was used to assess the expression of Runx2, osteocalcin, and collagen type 1 (COL1). Tangential sections were observed at 100× magnification for Runx2 and osteocalcin (scale bar: 200 µm), and at 400× for COL1 (scale bar: 50 µm).

Semi-quantitative analysis of IHC staining was conducted using the immunoreactive score (IRS), as detailed in Table 1. Serum samples were collected on days 0, 1, 3, 5, 7, 14, and 28 to quantify osteoprotegerin (OPG) levels using ELISA. Expression patterns of bone markers were compared with previously reported findings in nanocomposite scaffold models.

Statistical analysis

GraphPad Prism 8 (GraphPad Software, Boston, USA) statistical software was used for analysis. The data is expressed as mean ± standard deviation (SD). The significance of the differences between groups was tested using a nonparametric Kruskal–Wallis test or a parametric one-way ANOVA. The cutoff for statistical significance was set at $p<0.05$.

RESULTS

Characterization of the scaffold

The morphological analysis using scanning electron microscopy (SEM) revealed differences between the scaffolds (Fig. 1). BHA and nano-BHA exhibited spherical particles, with nano-BHA showing a smoother surface morphology. In contrast, calcium sulfate (CS) displayed irregular, non-spherical structures. The pore sizes of the scaffolds are presented in Table 2. The pore size of the nano-BHA scaffold was significantly larger than that of the BHA scaffold.

The elemental composition analysis via EDX is shown in Fig. 2. The Ca/P ratio of the nano-BHA scaffold (1.86) was closer to the physiological bone value of 1.67 compared to the BHA scaffold (1.98), as presented in Table 3. This suggests that the nano-BHA scaffold more closely mimics the mineral composition of native bone, a factor critical to scaffold integration. The osteoconductivity ratio of calcium to phosphorus is also an important factor when mimicking human bone. Ensuring the ratio is similar to that of the bone component increases the ability to heal the defect. The elemental spectra of nano-BHA and BHA scaffolds are shown in Fig. 2. The ratio of calcium to phosphorus in the nano-BHA scaffold was closer to the value of 1.67 seen in human bones than that of BHA, as shown in Table 3.

Effectiveness of the *in vivo* scaffold

Radiological observations were performed to observe the defects after treatment. A CT Scan figure of the femoral bone is shown in Fig. 3. The femoral bone on day 28 showed a smaller defect than that on day 7. The nano-BHA scaffold exhibited better defect closure than the BHA and defect models.

Following the previous result, hematoxylin and eosin (HE) staining of the bone tissue was performed to visualize the migration of the osteocytes, osteoblasts, and osteoclasts. These three types of bone cells are important for healing after a defect. The observations of these three cells are shown in Fig. 4. On day 7, bone matrix formation was absent in the control group but was observed in both scaffold groups. By day 28, more organized bone tissue was present, with the nano-BHA group displaying higher cellular activity. The quantitative analysis (Fig. 5) showed significantly higher numbers of osteoblasts, osteoclasts, and osteocytes in the nano-BHA group, indicating more advanced bone remodeling. Osteoclasts are involved in the bone remodeling process, where they resorb the broken bone matrix, followed by osteoblasts, which synthesize the new bone matrix. Meanwhile, osteocytes serve as tissue mechanosensors.

Table 1. Semi-quantitative immunoreactive score (Meyerholz and Beck, 2018).

A	B	AxB
0: no positive cell	0: no color after staining	0–1: negative
1: ≤10% positive cells	1: weak intensity	2–3: low
2: <10% and ≤50% positive cells	2: medium intensity	4–8: medium
3: <50% and >80% positive cells	3: strong intensity	9–12: high
4: ≥80% positive cells		

Table 2. Scaffold pore size.

Scaffold	Size Pore (µm)	Significance
Nano-BHA	0.613 ± 0.178	p=0.043
BHA	0.451 ± 0.152	

Table 3. Ratio of calcium and phosphorus in scaffolds.

Scaffold	Element concentration (%)		Ratio Ca/P
	Ca	P	
Nano-BHA	64.988	35.012	1.86
BHA	66.528	33.472	1.98

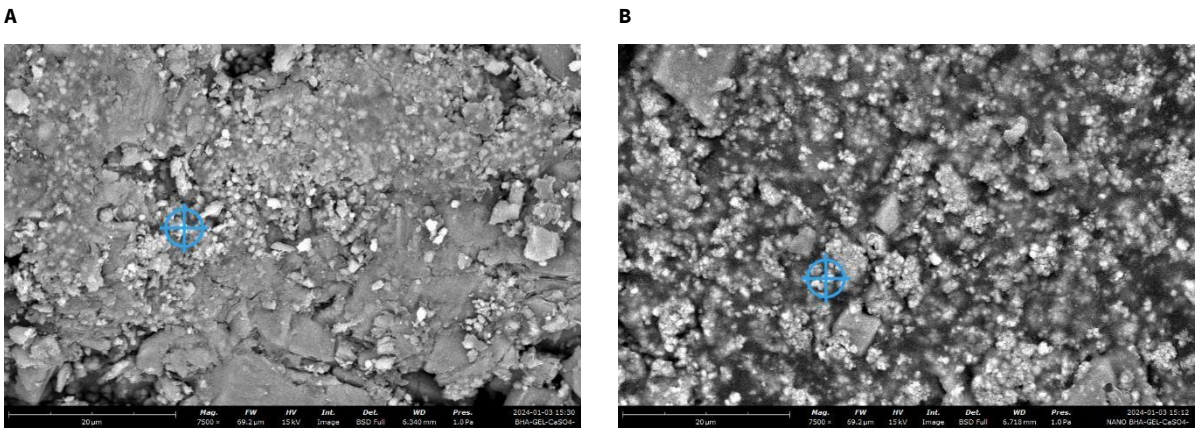

Figure1. Morphological observation of **(A)** bovine hydroxyapatite (BHA) scaffold and **(B)** nano-BHA scaffold using scanning electron microscopy (SEM) with 15,000× magnification.

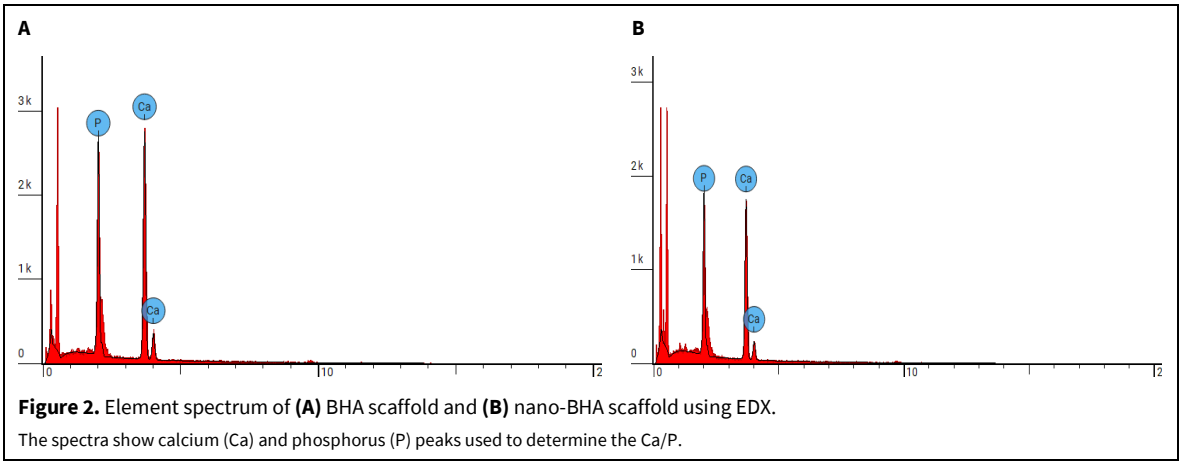

Figure 2. Element spectrum of **(A)** BHA scaffold and **(B)** nano-BHA scaffold using EDX.
The spectra show calcium (Ca) and phosphorus (P) peaks used to determine the Ca/P.

Runx2 expression, a marker of osteoblast differentiation, was evaluated by immunohistochemistry (Fig. 6). The nano-BHA group showed elevated expression of Runx2 on both day 7 and day 28, with immunoreactive scores (IRS) significantly higher than those in other groups (Fig. 7). Therefore, bone remodeling begins when osteoblasts form a new bone matrix.

Osteocalcin expression was also assessed (Fig. 8), revealing stronger signals in the nano-BHA group. Osteocalcin is secreted by mature osteoblasts and contributes to matrix mineralization. Higher IRS values in the nano-BHA group indicate more mature bone formation.

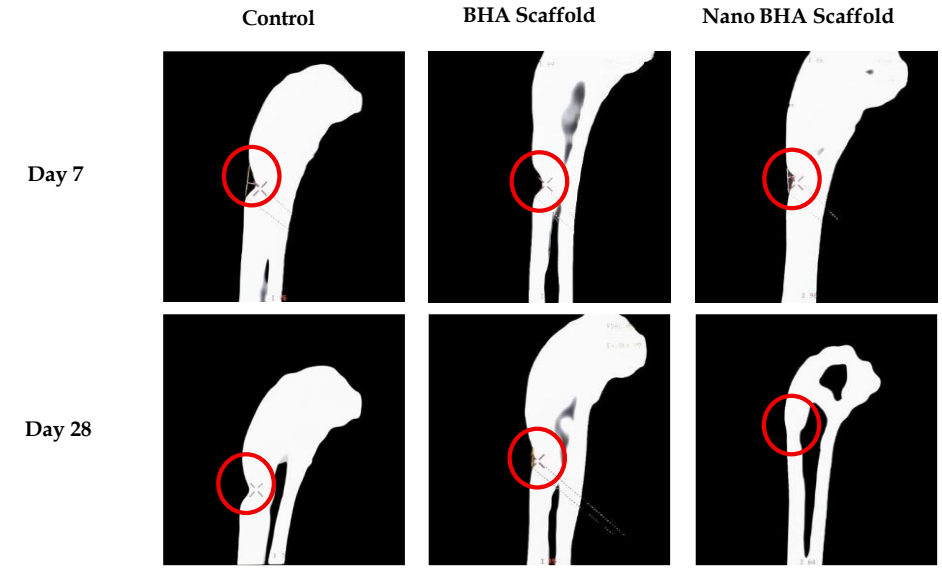

Figure 3. Computed tomography scans of femurs at days 7 and 28 post-implantation.

Red circles indicate the defect area in the femoral bone. The images show the progression of bone healing on days 7 and 28 across different treatment groups: Control, BHA scaffold, and nano-BHA. Notably, the nano-BHA group exhibits a smaller defect area, particularly on day 28, suggesting enhanced bone regeneration compared to the other groups.

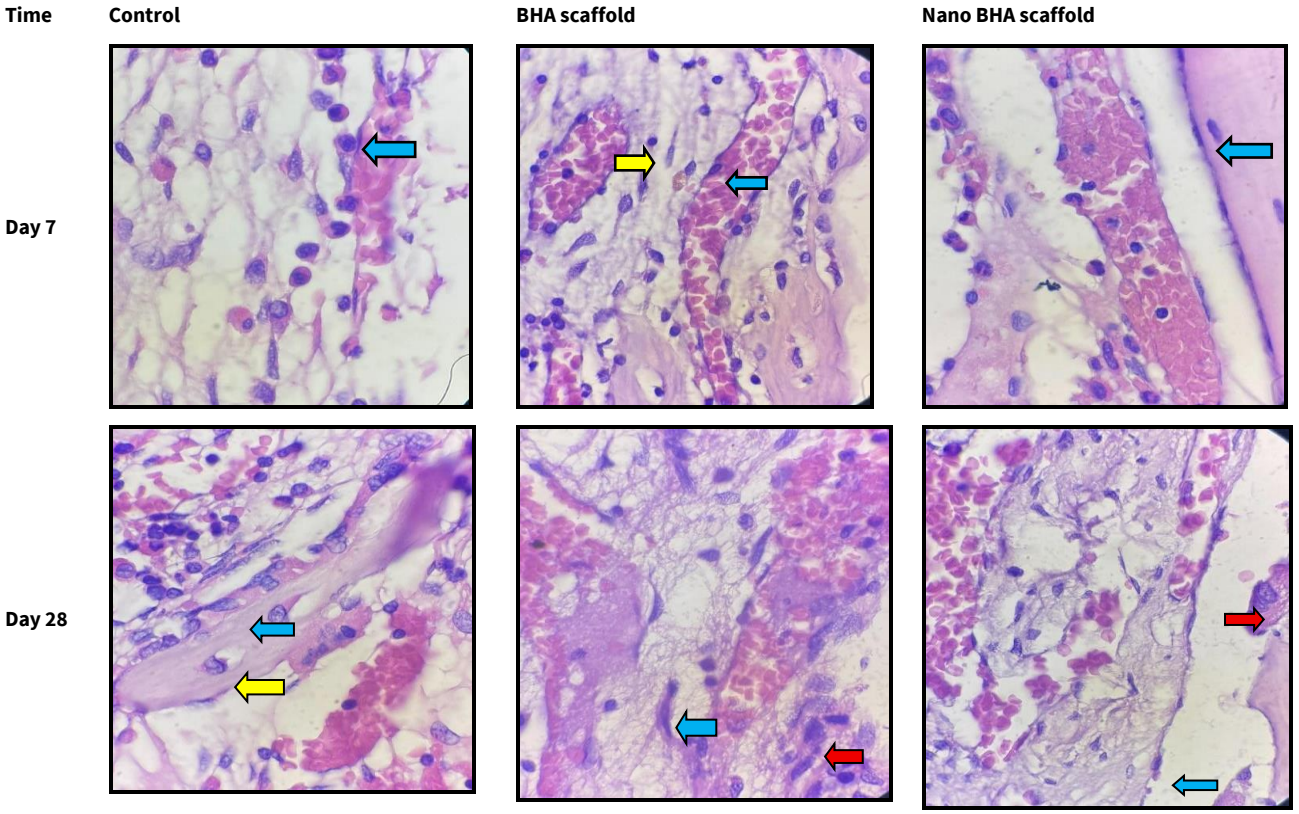

Figure 4. Hematoxylin and eosin (HE)-stained sections of femur tissue from each group on days 7 and 28.

Blue arrows indicate osteoblasts; yellow arrows indicate osteocytes; red arrows indicate osteoclasts; stars indicate the bone matrix. Scale bar 100× magnification = 200 µm.

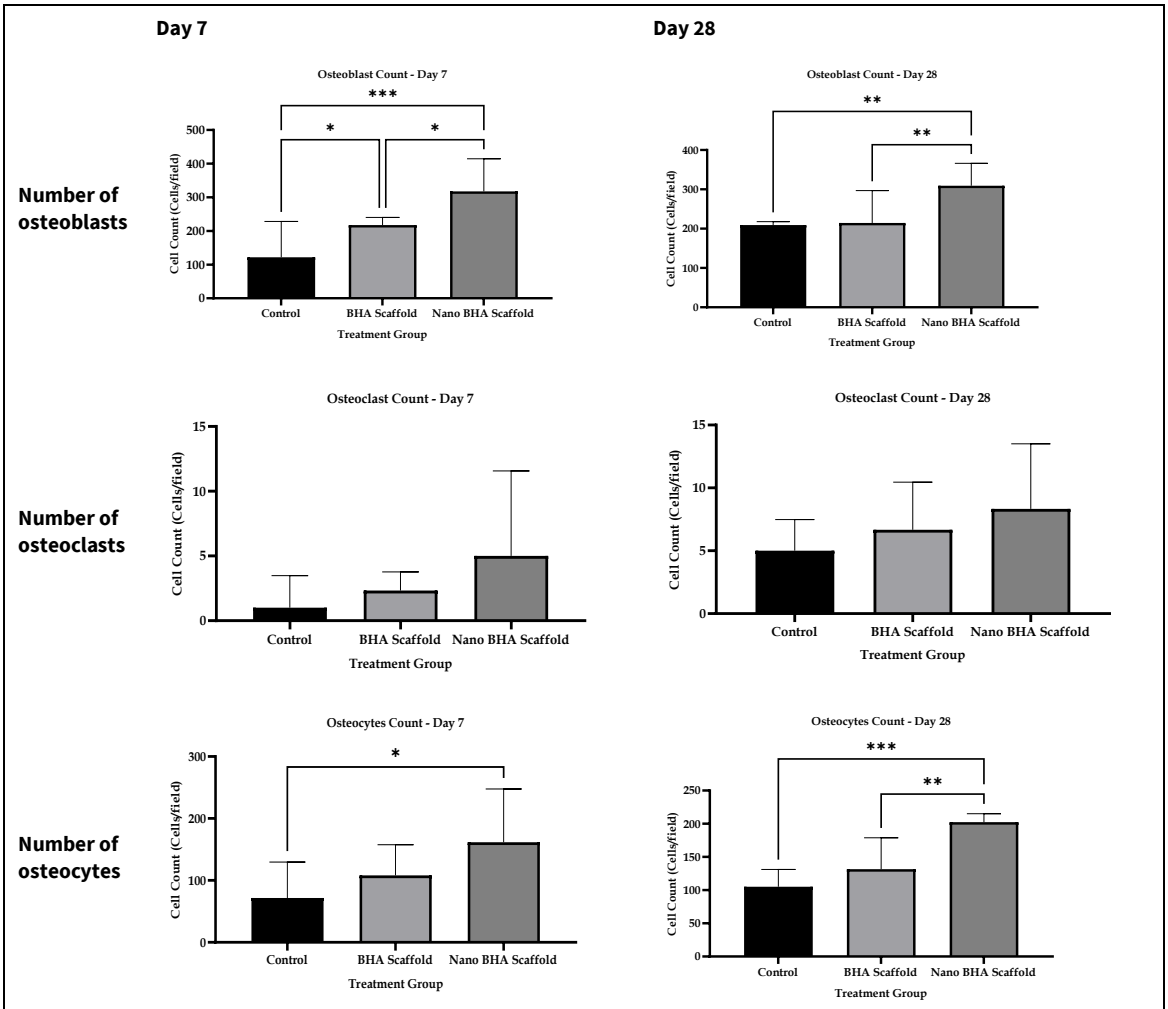

Figure 5. Quantitative analysis of osteoblasts, osteocytes, and osteoclasts per field at days 7 and 28 for each group.
Each bar represents the mean ± SEM (n=5). *p<0.05, **p≤0.01, ***p<0.001 based on a one-way ANOVA test.

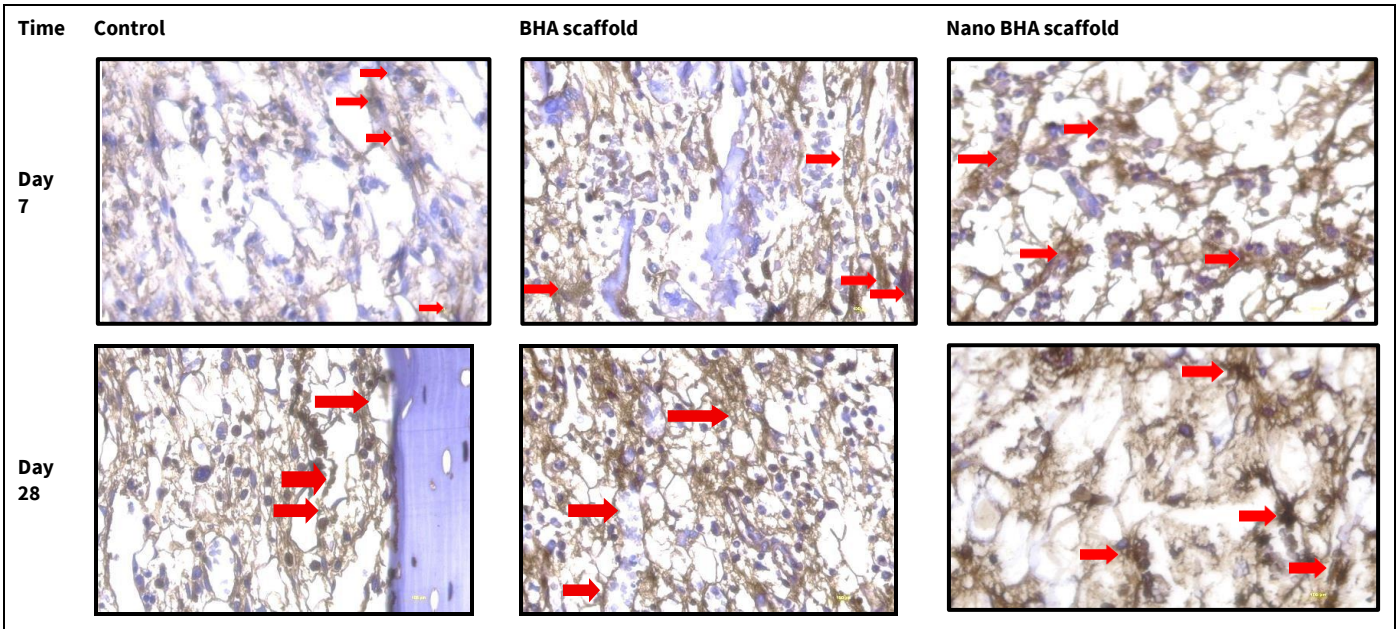

Figure 6. Immunohistochemical staining of Runx2 expression in femur sections from each group on days 7 and 28.
Red arrows mark the staining of Runx2. Scale bar 100× magnification = 200 µm.

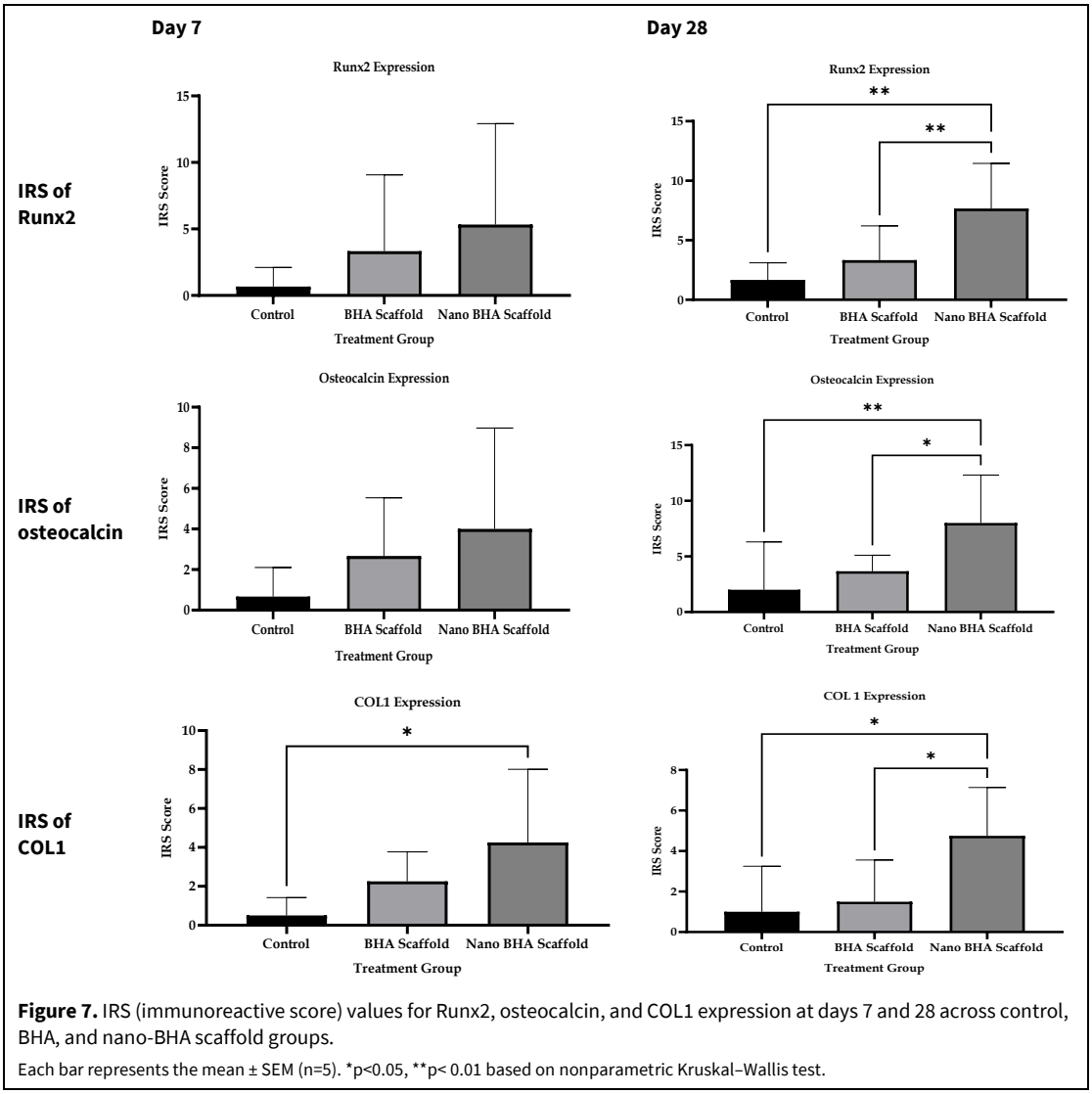

Figure 7. IRS (immunoreactive score) values for Runx2, osteocalcin, and COL1 expression at days 7 and 28 across control, BHA, and nano-BHA scaffold groups.

Each bar represents the mean ± SEM (n=5). *p<0.05, **p< 0.01 based on nonparametric Kruskal–Wallis test.

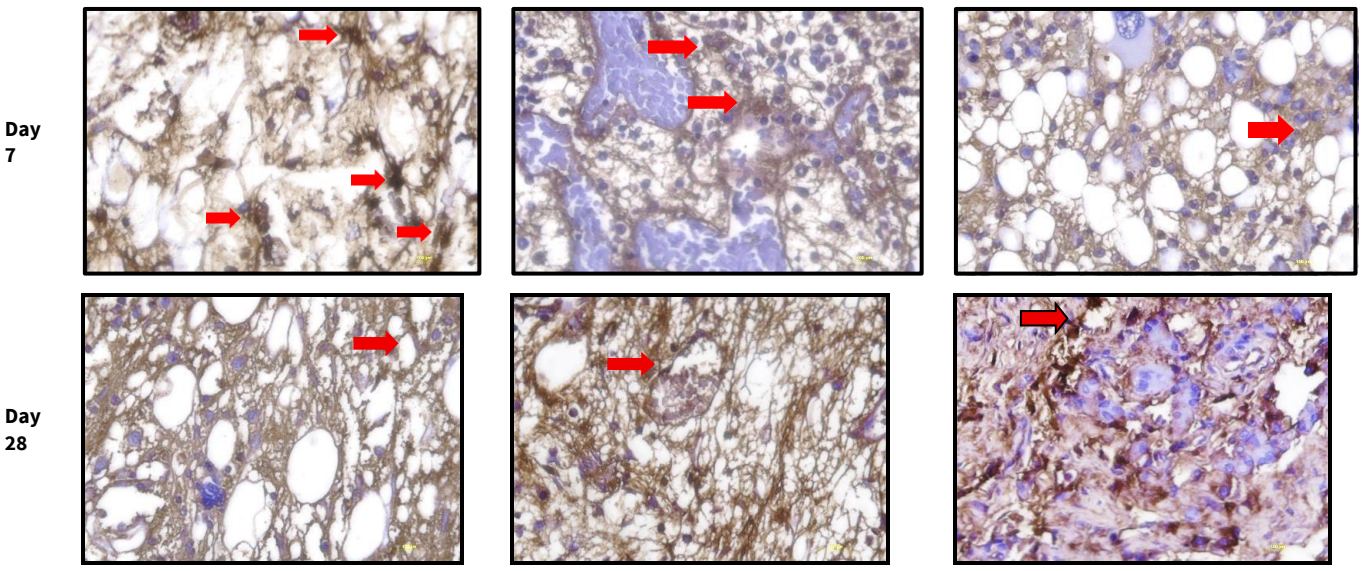

Figure 8. Immunohistochemical staining of osteocalcin expression in femur sections from each group on days 7 and 28.

Red arrows mark staining of osteocalcin. Scale bar 100× magnification = 200 µm.

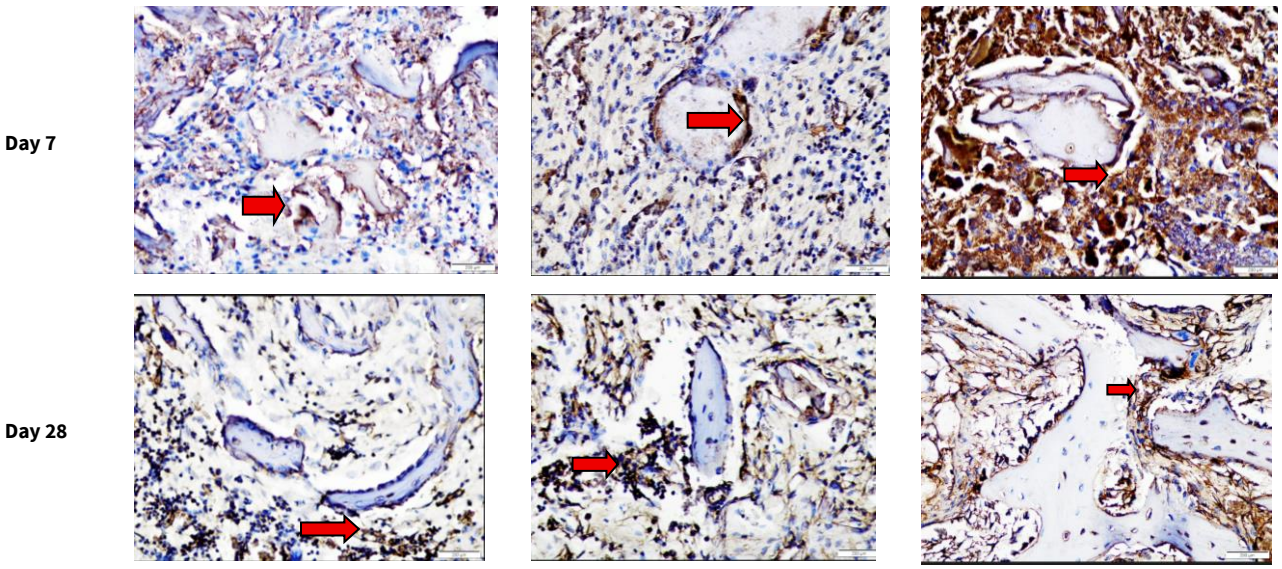

Figure 9. Immunohistochemical staining of collagen type I (COL1) expression in femur sections from each group on days 7 and 28.
Red arrows mark staining of COL1. Scale bar 400× magnification = 50 µm.

Type I collagen (COL1) accounts for approximately 90% of the extracellular matrix in bone tissue and plays a crucial role in maintaining bone structural integrity (Hatakeyama et al., 2013; Sardiñas et al., 2016). During the bone remodeling phase, preosteoblast differentiation is characterized by COL1 synthesis, which contributes to bone matrix mineralization. As shown in Fig. 9, COL1 immunostaining revealed more pronounced extracellular matrix formation in the nano-BHA scaffold group. Given that COL1 is the predominant collagen in bone, these findings suggest that the nano-BHA scaffold effectively promotes osteoblast maturation and matrix deposition.

The inflammatory phase is initiated by the recruitment of inflammatory cells that release proinflammatory cytokines. These cytokines activate osteoclasts and reduce serum levels of osteoprotegerin (OPG). OPG, a cytokine secreted by osteoblast-derived stromal cells, functions as a decoy receptor that inhibits osteoclastogenesis by preventing the interaction between RANKL and RANK (Kang et al., 2014), thereby suppressing osteoclast activation. As a result, osteoblast activity predominates over osteoclast activity, leading to increased bone formation. Elevated OPG levels indicate osteoclast inactivation, while reduced levels reflect osteoclast activation, marking the onset of the bone remodeling phase.

Serum OPG levels were monitored as biomarkers of osteoclast inhibition (Fig. 10). On day 14, the nano-BHA scaffold group showed a significantly higher OPG level than the BHA scaffold group ($p<0.05$), suggesting that the nano-BHA scaffold more effectively enhanced osteoblast activity and suppressed osteoclastogenesis.

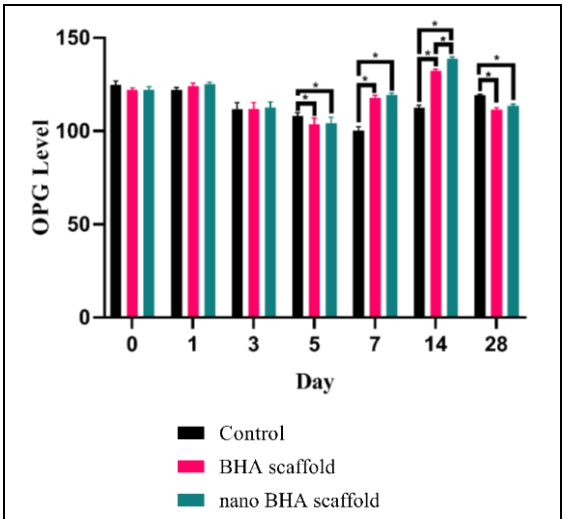

Figure 10. OPG levels in the fracture, BHA scaffold, and nano-BHA scaffold groups on days 0, 1, 3, 5, 7, 14, and 28.
Each bar represents the mean ± SEM (n=5). *p<0.05 based on a one-way ANOVA test.

DISCUSSION

BHA has been widely utilized as a bone implant material due to its inherent biocompatibility. The particle surface morphology, size distribution, and surface hydration level of nano-hydroxyapatite (nano-HA) have been reported to influence osteogenic responses significantly (Mastrangelo et al., 2013;

Tavakol et al., 2013). Nanoscale particles have been shown to enhance osteoblast proliferation, bone cell activity, and osseointegration more effectively than their micron-sized counterparts. Furthermore, the reduced particle size has been associated with increased calcium ion release, which may stimulate osteogenesis within scaffold pores (Li et al., 2016; Rogowska-Tylman et al., 2019).

Gelatin, a collagen-derived polymer, has been utilized to enhance the strength of BHA scaffolds due to its similarity to the bone extracellular matrix (Lee et al., 2013; Peng et al., 2015). Gelatin provides R-COO^- ions that interact with Ca^{2+} from HA, leading to the formation of nucleation sites essential for HA crystal development (Hu et al., 2018; Yue et al., 2022). Its incorporation has been reported to modulate scaffold degradation and enhance new bone synthesis.

CS is a resorbable material commonly applied in alloplastic grafts. Its degradation leaves no residual foreign matter and enables complete replacement with native bone. Released calcium ions are believed to stimulate osteoblastic activity and bone regeneration (Beuerlein and McKee, 2010). Upon degradation, CS creates an acidic microenvironment, potentially triggering bone remodeling by inducing cellular recruitment essential for this process (Yashavantha et al., 2013).

SEM analysis revealed spherical morphology for BHA and nano-BHA particles, while CS exhibited irregular chunk-like structures. The surface topography of the scaffolds was modified by CS addition, producing a rougher texture (Nicoara et al., 2023). The average pore diameter was greater in nano-BHA scaffolds than in BHA scaffolds, which may enhance vascularization and osteoblast function due to improved nutrient and oxygen diffusion (Abbasi et al., 2020). Elemental analysis indicated Ca/P ratios of 1.98 and 1.86 for BHA and nano-BHA scaffolds, respectively, which exceeded the stoichiometric ratio of 1.67 typical for natural bone (Loh and Choong, 2013). This discrepancy may result from CS-derived calcium content. Scaffolds mimicking native bone composition are considered beneficial for accelerating defect healing.

Based on CT scan observations, the *in vivo* efficacy test was conducted through a semi-quantitative analysis of bone defect gaps on days 7 and 28. Variations in the observed defect widths were noted visually. On day 7, narrower defect gaps were detected in the BHA and nano-BHA scaffold groups compared to the fracture control group. By day 28, defect gaps diminished further in the nano-BHA scaffold group. These observations suggest the potential integration of tissue into the scaffold, although this interpretation remains descriptive. Notably, statistical analysis did not reveal significant differences among the groups (Budiatin et al., 2022); therefore, no definitive conclusions could be drawn from the CT scan data alone.

Histological analysis using HE staining revealed enhanced cellular activity in animals receiving nano-BHA scaffolds. Accelerated migration of osteoblasts and osteoclasts was observed, accompanied by active matrix resorption and new matrix synthesis. This phenomenon was particularly pronounced on day 28, coinciding with increased osteoblast-to-osteocyte differentiation. Immunohistochemical staining for Runx2, osteocalcin, OCL1, and OPG also produced positive outcomes.

Runx2, a transcription factor essential for osteogenesis and fracture repair, was detected in high intensity within scaffold pores of the nano-BHA group on day 28. These regions exhibited dense infiltration of leukocytes and macrophages alongside the presence of nascent bone tissue surrounding residual scaffold material. Differentiated osteoblasts contributed to bone matrix formation, although areas of irregular mineralization were also noted. Preosteoblast proliferation and angiogenesis were evident in the regenerating tissue. Compared to native bone, newly formed tissue contained a higher density of osteoblasts, indicative of active bone remodeling (Raftery et al., 2017; Sivaraj and Adams, 2016). Osteoconductive properties of the nano-BHA scaffold were confirmed, along with the development of a fibrous capsule at the implant interface (Long, 2012; Ma'arif et al., 2022).

The role of Runx2 in terminal hypertrophic chondrocyte survival and differentiation into osteoblasts, which is vital for trabecular bone formation, was supported by observations on day 28 (Khotib et al., 2022). Signs of remodeling, including osteoblast differentiation and neovascularization, were confirmed via immunohistochemical analysis in both scaffold groups. These results underscore the regulatory function of Runx2 in osteoclast, osteoblast, and osteocyte activity, as well as macrophage-mediated modulation (Komori, 2018).

Osteocalcin, which facilitates osteoblast function, was actively absorbed in the scaffold regions, as confirmed by IHC. Its involvement in type I collagen fibrillogenesis and bone matrix mineralization was corroborated by the detection of mineralized osteoid produced by osteoblasts (Kenkre and Bassett, 2018). This process expedites the formation of structurally mature bone during repair. The presence of connective tissue, observed in IHC analysis, suggested ongoing secondary bone healing, particularly in unstabi-

lized defect zones. This healing process is driven by endochondral ossification, wherein mesenchymal cells differentiate into chondrocytes that deposit type II collagen matrix, later mineralized by osteoblasts (Bahney et al., 2019; Komori, 2020).

Elevated COL1 expression was detected in the nano-BHA scaffold group relative to the BHA and control groups at both time points, indicating enhanced osteoblast differentiation and matrix production. The osteoconductive environment promoted mesenchymal-to-osteoblast differentiation and facilitated type I collagen secretion for hard bone formation (Arufe et al., 2010; Gani et al., 2023).

By day 14, OPG levels were elevated in both scaffold groups, with a higher mean concentration in the nano-BHA scaffold group. The enhanced bioactivity of nanoscale BHA, attributed to improved dispersion and surface area, likely contributed to increased osteoblast proliferation and subsequent osteoprotegerin secretion. As osteoblast numbers increase, higher levels of this regulatory cytokine are produced, reinforcing bone formation and inhibiting osteoclastogenesis.

CONCLUSION

The reduced particle size of nano-BHA provides many advantages for its use as a scaffold for bone defect closure. In addition, the addition of calcium sulfate and gelatin enhances the scaffold's resemblance to natural bone composition. In this study, nano-BHA scaffold showed better homing properties than BHA scaffolds, as evidenced by the morphology of osteoblasts, osteoclasts, and osteocytes. The nano-BHA scaffolds exhibit good osteoconductive and osteoinductive properties, as evidenced by the upregulation of biological markers, including Runx2, osteocalcin, and type I collagen. The temporal profile of OPG levels showed that nano-BHA scaffolds can promote bone defect closure.

CONFLICT OF INTEREST

The authors declare no conflicts of interest.

ACKNOWLEDGMENTS

The authors thank the Lembaga Penelitian dan Pengabdian Masyarakat (LPPM) Universitas Airlangga and the Faculty of Pharmacy Universitas Airlangga. This research did not receive any specific grant from funding agencies in the public, commercial, or not-for-profit sectors.

REFERENCES

Abbasi N, Hamlet S, Love RM, Nguyen NT (2020) Porous scaffolds for bone regeneration. J Sci: Adv Mater Devices 5(1): 1–9. https://doi.org/10.1016/j.jsamd.2020.01.007

Adhikara AG, Maharani AP, Puspitasari A, Nuswantoro, NF, Juliadmi D, Maras MAJ, Nugroho DB, Saksono B, Gunawarman (2024) Bovine hydroxyapatite for bone tissue engineering: Preparation, characterization, challenges, and future perspectives. Eur Polym J 214: 113171. https://doi.org/10.1016/j.eurpolymj.2024.113171

Arufe MC, Fuente ADL, Fuentes I, Toro FJD, Blanco FJ (2010) Chondrogenic potential of subpopulations of cells expressing mesenchymal stem cell markers derived from human synovial membranes. J Cell Biochem 111(4): 834–845. https://doi.org/10.1002/jcb.22768

Azami M, Tavakol S, Samadikuchaksaraei A, Hashjin MS, Baheiraei N, Kamali M, Nourani MR (2012) A porous hydroxyapatite/gelatin nanocomposite scaffold for bone tissue repair: *In vitro* and *in vivo* evaluation. J Biomater Sci Polym Ed 23(18): 2353–2368. https://doi.org/10.1163/156856211X617713

Bahney CS, Zondervan RL, Allison P, Theologis A, Ashley JW, Ahn J, Miclau T, Marcucio RS, Hankenson KD (2019) Cellular biology of fracture healing. J Orthop Res 37(1): 35–50. https://doi.org/10.1002/jor.24170

Baino F, Novajra G, Vitale-Brovarone C (2015) Bioceramics and scaffolds: A winning combination for tissue engineering. Front Bioeng Biotechnol 3: 202. https://doi.org/10.3389/fbioe.2015.00202

Beuerlein MJS, McKee MD (2010) Calcium sulfates: What is the evidence? J Orthop Trauma 24(1): S46–S51. https://doi.org/10.1097/BOT.0b013e3181cec48e

Brahimi S, Ressler A, Boumchedda K, Hamidouche M, Kenzour A, Djafar R, Antunović M, Bauer L, Hvizdoš P, Ivanković H (2022) Preparation and characterization of biocomposites based on chitosan and biomimetic hydroxyapatite derived from natural phosphate rocks. Mater Chem Phys 276: 125421. https://doi.org/10.1016/j.matchemphys.2021.125421

Budiatin AS, Khotib J, Samirah S, Ardianto C, Gani MA, Putri BRKHP, Arofik H, Sadiwa RN, Lestari I, Pratama YA, Rahadiansyah E, Susilo I (2022) Acceleration of bone fracture healing through the use of Bovine Hydroxyapatite or Calcium Lactate oral and implant Bovine Hydroxyapatite – Gelatin on bone defect animal model. Polymers 14(22): 4812. https://doi.org/10.3390/polym14224812

Budiatin AS, Pramesti M, Nurfinti WO, Pratama YA, Ratri DMN, Ardianto C (2025) Effect of diclofenac sodium on the cartilage-regeneration potential of the chitosan-gelatin-chondroitin sulfate scaffold. Iraqi J Vet Sci 39(25): 243–251. https://doi.org/10.33899/ijvs.2024.153205.3865

Budiatin AS, Zainuddin M, Khotib J (2014) Biocompatible composite as gentamicin delivery system for osteomyelitis and bone regeneration. Int J Pharm Pharm Sci 6(3): 223–226.

Farbod K, Nejadnik MR, Jansen JA, Leeuwenburgh SCG (2014) Interactions between inorganic and organic phases in bone tissue as a source of inspiration for design of novel. Tissue Eng Part B 20(2): 173–188. https://doi.org/10.1089/ten.teb.2013.0221

Gani MA, Budiatin AS, Shinta DW, Ardianto C, Khotib J (2023) Bovine hydroxyapatite-based scaffold accelerated the inflammatory phase and bone growth in rats with bone defect. J Appl Biomater Funct Mater 21: 1–12. https://doi.org/10.1177/22808000221149193

Ghassemi T, Shahroodi A, Ebrahimzadeh MH, Mousavian A, Movaffagh J, Moradi A (2018) Current concepts in scaffolding for bone tissue engineering. Arch Bone Jt Surg 6(2): 90–99. https://doi.org/10.22038/abjs.2018.26340.1713

Ghiasi MS, Chen J, Vaziri A, Rodriguez EK, Nazarian A (2017) Bone fracture healing in mechanobiological modeling: A review of principles and methods. Bone Rep 6: 87–100. https://doi.org/10.1016/j.bonr.2017.03.002

Haris MS, Budiatin AS, Rahmadi M, Aryani T, Ramadhaniar M (2025) Fabrication and characterization of bone graft nano bovine hydroxyapatite-gelatine-calcium sulfate: A top-down approach for a natural biomaterial. Res J Pharm Technol 18(1): 326-2. https://doi.org/10.52711/0974-360X.2025.00051

Hatakeyama W, Taira M, Chosa N, Kihara H, Ishisaki A, Kondo H (2013) Effects of apatite particle size in two apatite/collagen composites on the osteogenic differentiation profile of osteoblastic cells. Int J Mol Med 32(6): 1255–1261. https://doi.org/10.3892/ijmm.2013.1516

Hu H, Huang BW, Lee YT, Hu J, Wong SW, Ko CC, You W (2018) Dramatic improvement of the mechanical strength of silane-modified hydroxyapatite–gelatin composites via processing with cosolvent. ACS Omega 3(3): 3592–3598. https://doi.org/10.1021/acsomega.7b01924

Jakubowska E, Bielejewski M, Milanowski B, Lulek J (2022) Freeze-drying of drug nanosuspension – Study of formulation and processing factors for the optimization and characterization of redispersible cilostazol nanocrystals. J Drug Delivery Sci Technol 74: 103528. https://doi.org/10.1016/j.jddst.2022.103528

Jokanović V, Čolović B, Marković D, Petrović M, Soldatović I, Antonijević D, Milosavljević P, Sjerobabin N, Sopta J (2017) Extraordinary biological properties of a new calcium hydroxyapatite/poly(lactide-co-glycolide)-based scaffold confirmed by *in vivo* investigation. Biomed Tech 62(3): 295–306. https://doi.org/10.1515/bmt-2015-0164

Kamal AF, Iskandriati D, Dilogo IH, Siregar NC, Hutagalung EU, Susworo R, Yusuf AA, Bachtiar A (2013) Biocompatibility of various hydroxyapatite scaffolds evaluated by proliferation of rat's bone marrow mesenchymal stem cells: An *in vitro* study. Med J Indones 22(4): 202–208. https://doi.org/10.13181/MJI.V22I4.600

Kang R, Luo Y, Zou L, Xie L, Lysdahl H, Jiang X, Chen C, Bolund L, Chen M, Besenbacher F, Bünger C (2014) Osteogenesis of human induced pluripotent stem cells derived mesenchymal stem cells on hydroxyapatite contained nanofibers. RSC Adv 4(11): 5734–5739. https://doi.org/10.1039/c3ra44181d

Kazimierczak P, Przekora A (2020) Osteoconductive and osteoinductive surface modifications of biomaterials for bone regeneration: A concise review. Coatings 10(10): 971. https://doi.org/10.3390/coatings10100971

Kementerian Kesehatan Republik Indonesia (2018) Laporan Nasional Riset Kesehatan Dasar. Kementerian Kesehatan RI.

Kenkre JS, Bassett JHD (2018) The bone remodelling cycle. Ann Clin Biochem 55(3): 308–327. https://doi.org/10.1177/0004563218759371

Khotib J, Marhaeny HD, Miatmoko A, Budiatin AS, Ardianto C, Rahmadi M, Pratama YA, Tahir M (2022) Differentiation of osteoblasts: the links between essential transcription factors. J Biomol Struct Dyn 41(19): 10257–10276. https://doi.org/10.1080/07391102.2022.2148749

Komori T (2018) Runx2, an inducer of osteoblast and chondrocyte differentiation. Histochem Cell Biol 149(4): 313–323. https://doi.org/10.1007/s00418-018-1640-6

Komori T (2020) Functions of osteocalcin in bone, pancreas, testis, and muscle. Int J Mol Sci 21(20): 7513. https://doi.org/10.3390/ijms21207513

Lambert F, Bacevic M, Layrolle P, Schüpbach P, Drion P, Rompen E (2017) Impact of biomaterial microtopography on bone regeneration: Comparison of three hydroxyapatites. Clin Oral Impl Res 28(10): e201–e207. https://doi.org/10.1111/clr.12986

Lee CY, Nedunchezian S, Lin SY, Su YF, Wu CW, Wu SC, Chen CH, Wang CK (2023) Bilayer osteochondral graft in rabbit xenogeneic transplantation model comprising sintered 3D-printed bioceramic and human adipose-derived stem cells laden biohydrogel. J Biol Eng 17(1): 74. https://doi.org/10.1186/s13036-023-00389-x

Lee JM, Choi BBR, Choi JH, Kim GC, Hwang DS, Chang MC, Byun JH, Kim UK (2013) Osteoblastic response to the hydroxyapatite/gelatin nanocomposite and bio-calcium phosphate cement. Tissue Eng Regener Med 10(2): 47–52. https://doi.org/10.1007/s13770-013-0344-1

Li J, Zhi W, Xu T, Shi F, Duan K, Wang J, Mu Y, Weng J (2016) Ectopic osteogenesis and angiogenesis regulated by porous architecture of hydroxyapatite scaffolds with similar interconnecting structure *in vivo*. Regener Biomater 3(5): 285–297. https://doi.org/10.1093/rb/rbw031

Loh QL, Choong C (2013) Three-dimensional scaffolds for tissue engineering applications: Role of porosity and pore size. Tissue Eng Part B 19(6): 485–502. https://doi.org/10.1089/ten.teb.2012.0437

Long F (2012) Building strong bones: molecular regulation of the osteoblast lineage. Nat Rev Mol Cell Biol 13(1): 27–38. https://doi.org/10.1038/nrm3254

Lu Y, Wang J, Yang Y, Yin Q (2021) Bone defects are repaired by enhanced osteogenic activity of the induced membrane: a case report and literature review. BMC Musculoskelet Disord 22: 447. https://doi.org/10.1186/s12891-021-04317-2

Lun D, Li S, Li N, Mou L, Li H, Zhu W, Li H, Hu Y (2024) Limitations and modifications in the clinical application of calcium sulfate. Front Surg 11: 1278421. https://doi.org/10.3389/fsurg.2024.1278421

Ma'arif B, Sholihah FA, Mahardiani A, Fauziyah B, Mirza DM, Agil M (2022) Runt-related transcription factor 2 (Runx2) measurement in phytoestrogen-induced bone: A comparison of western blot and immunohistochemistry methods. Biomed Pharmacol J 15(2): 1039–1052. https://doi.org/10.13005/bpj/2439

Mastrangelo F, Quaresima R, Grilli A, Tettamanti L, Vinci R, Sammartino G, Tetè S, Gherlone E (2013) A comparison of bovine bone and hydroxyapatite scaffolds during initial bone regeneration: An *in vitro* evaluation. Implant Dent 22(6): 613–622. https://doi.org/10.1097/ID.0b013e3182a69858

Meyerholz DK, Beck AP (2018) Principles and approaches for reproducible scoring of tissue stains in research. Lab Invest 98(7): 844–855. https://doi.org/10.1038/s41374-018-0057-0

Nicoara AI, Voineagu TG, Alecu AE, Vasile BS, Maior I, Cojocaru A, Trusca R, Popescu RC (2023) Fabrication and characterisation of calcium sulphate hemihydrate enhanced with Zn- or B-doped hydroxyapatite nanoparticles for hard tissue restoration. Nanomater 13(15): 2219. https://doi.org/10.3390/nano13152219

Peng H, Wang J, Lv S, Wen J, Chen JF (2015) Synthesis and characterization of hydroxyapatite nanoparticles prepared by a high-gravity precipitation method. Ceram Int 41(10): 14340–14349. https://doi.org/10.1016/j.ceramint.2015.07.067

Raftery RM, Castaño IM, Chen G, Cavanagh B, Quinn B, Curtin CM, Cryan SA, O'Brien FJ (2017) Translating the role of osteogenic-angiogenic coupling in bone formation: Highly efficient chitosan-pDNA activated scaffolds can accelerate bone regeneration in critical-sized bone defects. Biomaterials 149: 116–127. https://doi.org/10.1016/j.biomaterials.2017.09.036

Rogowska-Tylman, J, Locs J, Salma I, Woźniak B, Pilmane M, Zalite V, Wojnarowicz J, Kędzierska-Sar A, Chudoba T, Szlązak K, Chlanda A, Święszkowski W, Gedanken A, Łojkowski W (2019) *In vivo* and *in vitro* study of a novel nanohydroxyapatite sonocoated scaffolds for enhanced bone regeneration. Mater Sci Eng C 99: 669–684. https://doi.org/10.1016/j.msec.2019.01.084

Sardiñas C, Arreaza DD, Osorio H (2016) Changes in the proportions of types I and III collagen in hemorhoids: The sliding anal lining theory. J Coloproctol 36(3): 124–129. https://doi.org/10.1016/j.jcol.2016.04.003

Sivaraj KK, Adams RH (2016) Blood vessel formation and function in bone. Development (Cambridge) 143(15): 2706–2715. https://doi.org/10.1242/dev.136861

Smrke D, Rožman P, Veselko M, Gubina B (2013) Treatment of Bone Defects — Allogenic Platelet Gel and Autologous Bone Technique. In Regenerative Medicine and Tissue Engineering. IntechOpen https://doi.org/10.5772/55987

Song R, Murphy M, Li C, Ting K, Soo C, Zheng Z (2018) Current development of biodegradable polymeric materials for biomedical applications. Drug Des Dev Ther 12: 3117–3145. https://doi.org/10.2147/DDDT.S165440

Stewart S, Bryant SJ, Ahn J, Hankenson KD (2015) Bone Regeneration. In Translational Regenerative Medicine. Elsevier Inc., pp. 313–333. https://doi.org/10.1016/B978-0-12-410396-2.00024-4

Suyatno A, Nurfinti WO, Kusuma CPA, Pratama YA, Ardianto C, Samirah S, Rahadiansyah E, Khotib J, Budiatin AS (2024) Effectiveness of bilayer scaffold containing chitosan/gelatin/diclofenac and bovine hydroxyapatite on cartilage/subchondral regeneration in rabbit joint defect models. Adv Pharmacol Pharm Sci 2024: 6987676. https://doi.org/10.1155/2024/6987676

Tang D, Tare RS, Yang LY, Williams DF, Ou KL, Oreffo ROC (2016) Biofabrication of bone tissue: Approaches, challenges and translation for bone regeneration. Biomaterials 83: 363–382. https://doi.org/10.1016/J.BIOMATERIALS.2016.01.024

Tavakol S, Nikpour MR, Amani A, Soltani M, Rabiee SM, Rezayat SM, Chen P, Jahanshahi M (2013) Bone regeneration based on nano-hydroxyapatite and hydroxyapatite/chitosan nanocomposites: An *in vitro* and *in vivo* comparative study. J Nanopart Res 15: 1373. https://doi.org/10.1007/s11051-012-1373-8

Tsuchiya A, Sato M, Takahashi I, Ishikawa K (2018) Fabrication of apatite-coated gypsum granules and histological evaluation using rabbits. Ceram Int 44(16): 20330–20336. https://doi.org/10.1016/j.ceramint.2018.08.021

Ulery BD, Nair LS, Laurencin CT (2011) Biomedical applications of biodegradable polymers. J Polym Sci B: Polym Phys 49(12): 832–864. https://doi.org/10.1002/polb.22259

Yan TT, Wu SY, Fang M, Chen QH (2014) Research of preparation and properties of CaSO4/HAw bone graft substitute. Appl Mech Mater 707: 154–157. https://doi.org/10.4028/www.scientific.net/amm.707.154

Yashavantha KC, Nalini KB, Menon J, Patro DK, Banerji BH (2013) Calcium sulfate as bone graft substitute in the treatment of osseous bone defects, a prospective study. J Clin Diagn Res 7(12): 2926–2928. https://doi.org/10.7860/JCDR/2013/6404.3791

Yue Y, Xu P, Lei Z, Li K, Xu J, Wen J, Wang S, Cheng W, Lin S, Huang Z, Xu H (2022) Preparation and characterization of a novel drug-loaded bi-layer scaffold for cartilage regeneration. RSC Adv 12(16): 9524–9533. https://doi.org/10.1039/d2ra00311b

AUTHOR CONTRIBUTION:

Contribution	Pratama YA	Ananta IP	Haris MS	Maghfiroh N	Nabila H	Ardianto C	Rahmadi M	Khotib J	Hendradi E	Taher M	Mazidda S	Budiatin AS
Concepts or ideas								x	x			x
Design						x		x	x			x
Definition of intellectual content	x					x				x		x
Literature search	x		x	x	x	x			x	x	x	x
Experimental studies			x	x	x							
Data acquisition			x	x	x							
Data analysis		x	x	x	x	x	x	x	x	x		x
Statistical analysis			x	x	x					x		
Manuscript preparation	x	x					x	x			x	x
Manuscript editing	x	x					x	x			x	x
Manuscript review	x	x	x	x	x	x	x	x	x	x	x	x

Citation Format: Pratama YA, Ananta IP, Haris MS, Maghfiroh N, Nabila H, Ardianto C, Rahmadi M, Khotib J, Hendradi E, Taher M, Mazidda S, Budiatin AS (2025) Accelerated bone defect closure after administration of nano bovine hydroxyapatite-calcium sulfate-gelatin scaffold in bone defect models. J Pharm Pharmacogn Res 13(6): 1728–1741. https://doi.org/10.56499/jppres24.2310_13.6.1728

Publisher's Note: All claims expressed in this article are solely those of the authors and do not necessarily represent those of their affiliated organizations, or those of the publisher, the editors and the reviewers. Any product that may be evaluated in this article, or claim that may be made by its manufacturer, is not guaranteed or endorsed by the publisher.

Open Access: This article is distributed under the terms of the Creative Commons Attribution 4.0 International License (http://creativecommons.org/licenses/by/4.0/), which permits use, duplication, adaptation, distribution and reproduction in any medium or format, as long as you give appropriate credit to the original author(s) and the source, provide a link to the Creative Commons license and indicate if changes were made.

Supplementary Data

Appendix A. The formula of the scaffold.

Table 1. The formula of scaffolds.

No	Nano BHA scaffold		BHA scaffold	
	Material	**Quantity**	**Material**	**Quantity**
1	Nano BHA	515 mg	BHA	515 mg
2	Calcium sulfate dihydrate	385 mg	Calcium Sulfate Dihydrate	385 mg
3	Gelatine	100 mg	Gelatine	100 mg

Appendix B. ARRIVE 2.0 essential 10 checklist.

Title of Study: Accelerated Bone Defect Closure After Administration of Nano Bovine Hydroxyapatite-Calcium Sulfate-Gelatin Scaffold in Bone Defect Models

Item	ARRIVE Essential 10 Item	Description and Location in Manuscript
1	Study Design	A randomized, controlled *in vivo* study with three groups (control, BHA scaffold, nano-BHA scaffold). The experimental unit was one rabbit. *(Materials and Methods – Animals)*
2	Sample Size	A total of 30 rabbits (n=10/group) were used. No formal sample size calculation was conducted; the group size was based on prior studies with similar endpoints. *(Materials and Methods – Animals)*
3	Inclusion/Exclusion Criteria	Rabbits were aged 4–8 months, weighed 2.0–3.0 kg, and were healthy. No animals or data were excluded after allocation. *(Materials and Methods – Animals)*
4	Randomisation	Animals were allocated to groups using computer-generated randomization. Allocation was performed by a researcher independent of the analysis. *(Materials and Methods – Animals)*
5	Blinding	Outcome assessments (histology, IHC, ELISA) were performed blinded to group assignment. *(Materials and Methods – Characterization)*
6	Outcome Measures	Primary outcomes: osteogenic marker expression and cell migration. Secondary outcomes: CT-based defect closure, serum OPG levels. *(Materials and Methods – In Vivo Effectiveness; Results)*
7	Statistical Methods	Data were analyzed using one-way ANOVA and Kruskal–Wallis tests. Normality and variance homogeneity were tested using Shapiro–Wilk and Levene's tests, respectively. *(Statistical Analysis)*
8	Experimental Animals	Species: New Zealand White rabbit; female; 4–8 months; 2.0–3.0 kg. *(Materials and Methods – Animals)*
9	Experimental Procedures	Scaffold fabrication, surgical bone defect creation, implantation, and postoperative care are described. Imaging and staining protocols are specified. *(Materials and Methods – Scaffold Preparation; Procedures)*
10	Results	Data are presented with n values, means ± SEM, p-values. Differences between groups are statistically tested. *(Results and Discussion)*

Additional ARRIVE Details for Transparency:

- **Randomization and Allocation:** Group allocation was randomized using a digital randomization tool and conducted by a researcher not involved in the analysis.
- **Blinding:** Histological, IHC, and biochemical analyses were carried out by investigators blinded to treatment groups.
- **Housing and Husbandry:** Rabbits were housed in temperature-controlled rooms (22 ± 2°C) with a 12-h light/dark cycle. Acclimatization lasted 7 days. Animals had ad libitum access to food and water.
- **Inclusion/Exclusion Details:** No animals were excluded after group allocation. All data points were included in the analysis.
- **Statistical Assumptions:** Data normality was confirmed using the Shapiro–Wilk test, and variance equality was assessed using Levene's test.
- **Effect Sizes and CI:** Results were expressed as means ± SEM. Effect sizes or confidence intervals were not calculated but will be considered in future studies.

This checklist has been completed in accordance with the ARRIVE 2.0 guidelines to ensure transparency and reproducibility in animal research reporting.